Thermochemistry and phase stability of the polymorphs of yttrium tantalate, YTaO$_4$

Maren Lepple[1,4,*], Sergey V. Ushakov[2], Kristina Lilova[2],

Chandra A. Macauley[3,5], Abel N. Fernandez[3,6], Carlos G. Levi[3], Alexandra Navrotsky[2]

[1] Eduard-Zintl-Institut für Anorganische und Physikalische Chemie, Technische Universität Darmstadt, Darmstadt, Germany

[2] School of Molecular Sciences and Center for Materials of the Universe, Arizona State University, Tempe, AZ 85287, USA

[3] Materials Department, University of California Santa Barbara, Santa Barbara, CA, USA

[4] presently Senior Scientist at DECHEMA Forschungsinstitut, Frankfurt, Germany

[5] presently Senior Scientist in the Department of Materials Science and Engineering (Institute I) at Friedrich-Alexander-Universitaet, Erlangen-Nuernberg, Germany

[6] presently graduate student in the Department of Materials Science and Engineering at University of California Berkeley, Berkeley, CA, USA

*corresponding author, contact details: maren.lepple@dechema.de, Theodor-Heuss-Allee 25, 60486 Frankfurt am Main, Germany, telephone: +49 69 7564439, fax: +49 69 7564388

Abstract

Thermodynamic parameters of the three fergusonite-related polymorphs M', M and T of YTaO$_4$ and their phase stabilities were investigated experimentally. The debate on the relative stability of the M and M' phases was resolved, and it was shown that the compound does not transform to a cubic polymorph prior to melting. The enthalpies of formation of M and M' were determined using high temperature oxide melt solution calorimetry, and the heat capacities and heat contents were measured. The enthalpy of the M' to T phase transition was measured by differential thermal analysis. The stability of the T phase up to its melting at 2090 °C was demonstrated using high temperature X-ray diffraction and thermal analysis. Its enthalpy of fusion was determined using drop-and-catch calorimetry. The thermodynamic properties of YTaO$_4$ assessed in this study enable the thermodynamic modeling of its polymorphs and related materials systems of technological importance.

Keywords: yttrium tantalate, YTaO$_4$, oxide materials, thermodynamic properties, thermal analysis, calorimetry, synchrotron radiation

1.   Introduction

Compositions in the ZrO$_2$-Y$_2$O$_3$-Ta$_2$O$_5$ system are of interest for applications as diverse as phosphors [1,2], microwave dielectrics [3], lasers [4], catalysis [5], fuel cells [6,7] and next generation thermal barrier coatings (TBCs) [8], which motivated recent investigations into the phase equilibria in this system [9,10]. Key features of the system are a ZrO$_2$-rich tetragonal solid solution phase field that is stable to at least 1500 °C and is obtained by equimolar co-doping of Y^{3+} and Ta^{5+}, as well as a YTaO$_4$ phase field that has substantial solubility for Zr^{4+} substituting equally in each cation lattice [8–13]. Compared to the state-of-the-art TBC material, yttria stabilized zirconia (8YSZ), YTaO$_4$ has lower thermal conductivity [13,14] and a similar thermal expansion coefficient [15]. While YTaO$_4$ is nominally phase stable below ~1450 °C, it undergoes a ferroelastic phase transition when cooled from above this temperature [16,17]. However, this transformation does not have a deleterious volume expansion like the tetragonal to monoclinic transformation in YSZ so it should not compromise the mechanical integrity of the coating [13,15,17].

YTaO$_4$ has three fergusonite-related polymorphs: (i) the monoclinic M' structure with space group P2/a that is reportedly stable from room-temperature to ~ 1450 °C [18], (ii) another monoclinic structure M with space group I2 that is isostructural with the mineral fergusonite [19,20] and it also appears stable at room temperature, and (iii) the high temperature tetragonal scheelite-type T structure with space group I4$_1$/a [19]. It is still under debate which of the two monoclinic phases is the thermodynamically stable room temperature phase. M' YTaO$_4$ can be synthesized at temperatures below the M' to T transformation, which is reconstructive and relatively sluggish [18]. In consequence, the transformation temperatures reported in the literature differ depending on the measurement technique, heating rate, and sample synthesis. Reported transition temperatures include 1450-1460 °C [1] and 1425-1450 °C [21] based on X-ray diffraction (XRD) after heat treatments, 1500 °C by differential thermal analysis (DTA), and 1438 °C by differential scanning calorimetry (DSC) [11]. Upon cooling from the tetragonal phase, YTaO$_4$ resists transformation back to M' but forms instead the monoclinic M phase by a displacive ferroelastic transformation proposed to be second-order [1,18,19] at 1426 ± 7 °C [17]. Therefore, M YTaO$_4$ can only be synthesized via the tetragonal high temperature phase and by inference M' should be the stable phase at room temperature [1]. Recent first principles computations tackled the question of phase stability and also proposed M' YTaO$_4$ to be the equilibrium low temperature phase [22,23]. However, the energies of M' and M were very close and their difference was calculated to be less than 10 meV/atom (0.6 kJ/mol) at 0 K [22].

YTaO$_4$ has been reported to melt congruently at 2044 ± 50 °C [24]. No other high temperature phase transitions above 1500 °C have been reported. However, Gurak *et al.* [12] suggested that a cubic fluorite-related phase is likely to be stable above 1700 °C due to the structural similarities of T YTaO$_4$ and t ZrO$_2$.

Recent studies in the ZrO$_2$-Y$_2$O$_3$-Ta$_2$O$_5$ system [9–12,22,25] focused on characterization of the phases, phase relations and properties such as thermal conductivity [13,14]. However, it is essential to have a complete thermodynamic description of the system for high temperature applications such as TBCs. This would allow understanding of the energies of the stable and metastable phases and the driving forces to predict long term phase evolution and reactivity with other materials. Missing thermodynamic data for the YTaO$_4$ phases and for other compounds in the ZrO$_2$-Y$_2$O$_3$-Ta$_2$O$_5$ system severely limit the accuracy of the thermodynamic assessment of this system, e.g. that performed by Bhattacharya *et al.* [26]. In that assessment, the phase transitions of YTaO$_4$ were not considered and a single phase was assumed to be stable from room temperature to the melting point with a heat capacity described as the sum of the heat capacities of the constituent oxides. These assumptions contributed to phase field shapes that are inconsistent with experimental observations [8,9,27]. A more recent study measured the low temperature heat capacity of M' YTaO$_4$ and subsequently derived the thermodynamic functions of this phase [28]. Based on this data, the investigation of the phase equilibria in the Y$_2$O$_3$-Ta$_2$O$_5$ quasibinary system by Fernandez et al. [25] and own additional DFT calculations, Zhang et al. modeled this system using the CALPHAD technique [23].

The purpose of this investigation is to experimentally determine the thermodynamic parameters (enthalpies of formation, phase equilibria, transition temperatures and enthalpies associated with the different polymorphs) of YTaO$_4$. The energetics and phase stabilities of YTaO$_4$ have been measured using high temperature oxide melt solution calorimetry, differential scanning calorimetry (DSC), differential thermal analysis (DTA), measurement of cooling traces using laser melting, drop calorimetry on laser heated aerodynamically levitated samples and X-ray diffraction, both *in situ* (high temperature) and after thermal exposure.

2.   Experimental methods

2.1.   *Sample Synthesis*

Powders of YTaO$_4$ were synthesized using reverse co-precipitation [9]. Precursor solutions of yttrium nitrate hexahydrate (99.9 % rare earth oxide basis, Alfa Aesar) in deionized water and tantalum chloride (99.99 % trace metals basis, ACROS-organics) in ethanol, calibrated by gravimetric means, were mixed in a Y^{3+}:Ta^{5+} cation ratio of 1:1. The mixed

solution was added dropwise into ammonium hydroxide, and the pH was maintained to be greater than 10 to ensure precipitation of all cations. The precipitates were filtered, washed with ethanol and dried overnight at 100 °C, followed by calcination at 900 °C for 4 h in a box furnace in air. Subsequently, the powders were heat treated for 100 h in air at 1250 °C or 1500 °C to yield M' $YTaO_4$ and M $YTaO_4$, respectively. A sample of M' from a separate batch containing a minor amount of YTa_3O_9 was heat treated for 2 h at 1500 °C, cooled to 1210 °C and held for 2h to convert it to M. It was then heat treated at 1400 ± 5 °C for 100 h, together from an M' sample of the same batch, to assess the relative stability of the two monoclinic phases.

YTaO4 was also synthesized by solid-state reaction from the pure oxides. Y_2O_3 (99.9% purity Alfa Aesar) and Ta_2O_5 (99.5 % purity, Alfa Aesar) were ball milled in ethanol using YSZ milling media for 48 h. The resulting slurry was dried overnight and then heat treated at 1500 °C for 100 h in air.

Laser melted beads of the ball milled powder were produced using a 400 W CO_2 laser (Firestar i401, Synrad, Mukilteo, WA) as described in [29]. The powder was placed in a copper hearth cavity in air under the laser beam and the laser power was increased manually until the powder melted. When the laser was turned off, the melt solidified in a spherical shape surrounded by the residual powder, which did not melt during the process (so called self-crucible conditions) [29]. These samples were laser-remelted in the aerodynamic levitator before analysis.

2.2. Crystal structure, microstructure and microchemical characterization

The phase composition of the samples was characterized using X-ray powder diffraction (XRD) and the Rietveld method. The XRD measurements were carried out on a STOE Stadi P diffractometer (linear PSD) with $CuK_{\alpha 1}$ radiation (Ge monochromator, λ = 1.540598 Å) in transmission geometry in a 2θ range between 10° and 90°. The GSAS-II software [30] was used for the Rietveld analysis of the diffraction patterns.

A laser-melted bead was polished to 0.01 μm embedded in conducting clay and then coated with a 5 nm Pt/Pd film to ensure electronic conductivity of the surface. The morphology was characterized using a BSD4 backscatter electron (BSE) detector in a Crossbeam 540 Gemini II scanning electron microscope (SEM) (Carl Zeiss Microscopy GmbH, Germany).

The crucibles from thermal analysis were cut in half and mounted in epoxy resin before they were ground and polished to 1 μm and coated with carbon to render the surfaces electrically conductive. The morphology was characterized using a XL40 SEM (Philips, Netherlands) equipped with BSE and an energy dispersive x-ray spectrometer (EDX) (EDAX, USA).

2.3. *In situ high temperature synchrotron X-ray diffraction*

High temperature diffraction experiments on YTaO$_4$ up to the melting temperature were performed on an aerodynamic levitator at the beamline 6-ID-D at the Advanced Photon Source (APS) as described earlier [31]. The laser-melted YTaO$_4$ bead of approximately 2.5 mm in diameter was levitated in oxygen flow; the flow rate was adjusted to ensure rotation of the bead necessary to obtain powder like diffraction patterns. The diffraction images were collected with a wavelength of 0.1236 Å in a Debye-Scherrer geometry as a sum of 100 exposures of 0.1 s of a Perkin-Elmer XRD 1621 area detector. The sample to detector distance was calibrated using CeO$_2$ powder glued to the surface of a ~ 2 mm Styrofoam sphere and with a Y$_2$O$_3$ bead prepared by laser melting. For the refinement of the high temperature XRD data from the YTaO$_4$ bead, sample displacement parameters were refined for the bead levitated at room temperature by fixing the cell parameters to the known value and were kept constant during the refinements of the high temperature patterns (see section 2.2).

Diffraction patterns were taken in 100 °C steps starting from 1000 °C as measured on top of the laser heated bead with a single-color pyrometer (IR-CAS3CS, Chino Co., Tokyo, Japan, emissivity set to 0.92). However, the emissivity is not known for the different phases of YTaO$_4$ at this temperature range, oscillations of the sample in the pyrometer field and a thermal gradient in the levitated sample heated by the laser from the top [32] impede an accurate temperature determination during the experiment. Thus, as in previous studies using this method [31,33,34], the temperature of diffracted volume is calibrated based on known temperatures of phase transformations. Therefore, for calculations of the thermal expansion, the largest lattice parameter of the tetragonal T YTaO$_4$ phase coexisting with melt was assigned to be the melting temperature (2090 °C), and the smallest lattice parameter coexisting with monoclinic phase was assigned to be the M→T transition temperature (1426 °C [17]).

From the refined lattice parameters, the coefficients of thermal expansion α of the lattice parameters l of the high temperature phase T were calculated using the following equation

$$\alpha = \frac{l_{2090°C} - l_{1426°C}}{l_{1426°C}} \cdot \frac{1}{\Delta T} \tag{1}$$

where $l_{2090°C}$ and $l_{1426°C}$ are the lattice parameters of the tetragonal phase as defined above and ΔT is the temperature difference. The isotropic coefficient of thermal expansion was derived using the refined Volume V applying the following equation

$$\langle \alpha \rangle = \frac{1}{3} \cdot \frac{V_{2090°C} - V_{1426°C}}{V_{1426°C}} \cdot \frac{1}{\Delta T} \tag{2}$$

2.4.   *Drop-and-catch (DnC) calorimetry*

The fusion enthalpy was determined using drop-and-catch calorimetry (DnC). The design of the instrument and calibration of the calorimeter are described in detail in [29,35,36]. Experiments were performed on YTaO$_4$ beads, ~70 mg in weight, prepared by laser melting of the ball-milled powder. The beads were levitated in oxygen flow in a splittable-nozzle aerodynamic levitator, heated with a 400 W CO$_2$ laser and then dropped into a heat flow calorimeter at 25 °C. The surface temperature of the bead before the drop was measured using a spectro-pyrometer (FAR Associates, Macedonia, OH, USA). The enthalpy of fusion was derived from the step in the enthalpy curve resulting from experiments on the samples caught in a molten and solid state. Due to the sample cooling during the ~100 ms drop time, it was necessary to heat the beads to more than 200 °C above the melting temperature of YTaO$_4$ to catch the sample in the liquid state. The sample was weighed on a microbalance after each drop to detect possible sample loss from evaporation, which did not exceed 0.01 mg (< 0.02 %).

2.5.   *Thermal analysis and differential scanning calorimetry*

High temperature differential thermal analysis (DTA) was performed using a SetSys 2400 instrument (Setaram, Cailure, France) using W-WRe sensor and thermocouples. The measurements were conducted in W crucibles using Ar flow (purity 99.999, 40 ml/min) and 20 °C/min heating and cooling rates. For the experiments above 1700 °C, the crucibles were sealed in Ar atmosphere using a tungsten inert gas (TIG) welding procedure to avoid carbon contamination from the vitreous carbon furnace protection tube. The phase transformation temperatures were determined with the method of first deviation from the baseline [37] and temperature and sensitivity calibrations were performed from fusion enthalpies and melting temperatures of Au, α-Al$_2$O$_3$ and Y$_2$O$_3$ standards as described elsewhere [35].

DTA experiments were limited to a moderately reducing environment due to the use of W crucibles. Solidification of YTaO$_4$ was also studied by recording cooling traces of laser melted samples levitated in oxygen flow. After melting the sample, the 400 W CO$_2$ laser was turned off while the surface temperature of the sample was measured with the spectropyrometer. The solidification temperature was determined from the maximum temperature of the recalescence peak.

Differential scanning calorimetry (DSC) was used to determine the heat capacities of M' and M YTaO$_4$ at 100 – 800 °C at a heating rate of 10 °C/min. The measurements were performed in an STA 449 F3 Jupiter instrument (Netzsch, Selb, Germany) using Pt/Rh crucibles in Ar atmosphere (purity 99.999, 50 ml/min). The measurements were conducted following the

standard IUPAC protocol [38], starting with a baseline measurement, followed by a reference measurement using a sapphire disc with known mass and then the sample measurement with a pressed powder sample with a diameter of 5 mm and a similar thermal mass as the sapphire disc.

2.6. *High temperature oxide melt solution calorimetry*

High temperature calorimetry was performed at 701 °C using a custom-built Calvet calorimeter as described in [39,40]. Drop solution experiments were conducted to determine the standard enthalpies of formation of M' and M YTaO$_4$. Sodium molybdate melt (3Na$_2$O·4MoO$_3$) was used as a solvent, synthetic air (80%N$_2$/20%O$_2$) gas with a flow rate of 6 ml/min was bubbled through the solvent to help dissolution of the gently pressed samples. Additionally, air was flushed over the melt with a rate of 35 ml/min. Approximately 5 – 8 mg samples were dropped into 20 g solvent. The measured heat effect, called the drop solution enthalpy, consists of the heat content of the compound from room temperature to 701 °C and the enthalpy of solution.

Transposed temperature drop experiments measured the enthalpy increments of M' and M YTaO$_4$ between room temperature and calorimeter temperature. The samples in form of 8 – 10 mg pellets were dropped from room temperature into an empty Pt crucible in the calorimeter at 701 °C.

3.   Results

3.1. *Phase characterization at room temperature*

Samples from different synthesis routes were characterized using XRD and the refined unit cell parameters are given in Table 1. The sample synthesized using co-precipitation and heat treated at 1250 °C shows pure M' phase, whereas both the co-precipitated and the solid-state synthesized materials show pure M phase after heating at 1500 °C. The additional M and M' samples described in Section 2.1 were heat treated at 1400 ± 5 °C for 100 h to assess their relative stability just below their reported transformations to the T phase. The M' phase persisted during this treatment whereas the M phase transformed to M', confirming the latter is the stable lower temperature polymorph of YTaO$_4$. The XRD patterns are given in Figure 1.

Table 1: Phases and refined unit cell parameters of the differently synthesized
YTaO$_4$ samples heat treated at different temperatures.

Synthesis Route	Co-precipitation		Ball Milling	Laser Melting
Condition	1250 °C/100 h/air	1500 °C/100 h/air		Flowing O$_2$
Phase/Space Gr	M' / $P2/a$	M / $I2$		
Unit cell – a (Å)	5.2952(2)	5.32564(5	5.32096(6)	5.3248(2)
Unit cell – b (Å)	5.46047(9)	10.93061(6)	10.92164(7)	10.9229(2)
Unit cell – c (Å)	5.1082(2)	5.05324(5)	5.04891(6)	5.0524(1)
Unit cell – β (°)	96.329(2)	95.5251(4)	95.5160(5)	95.4502(8)
UC Volume (Å^3)	146.7997	292.7951	292.0517	292.5305
Molar Vol (cm^3)	44.20	44.08	43.97	44.04
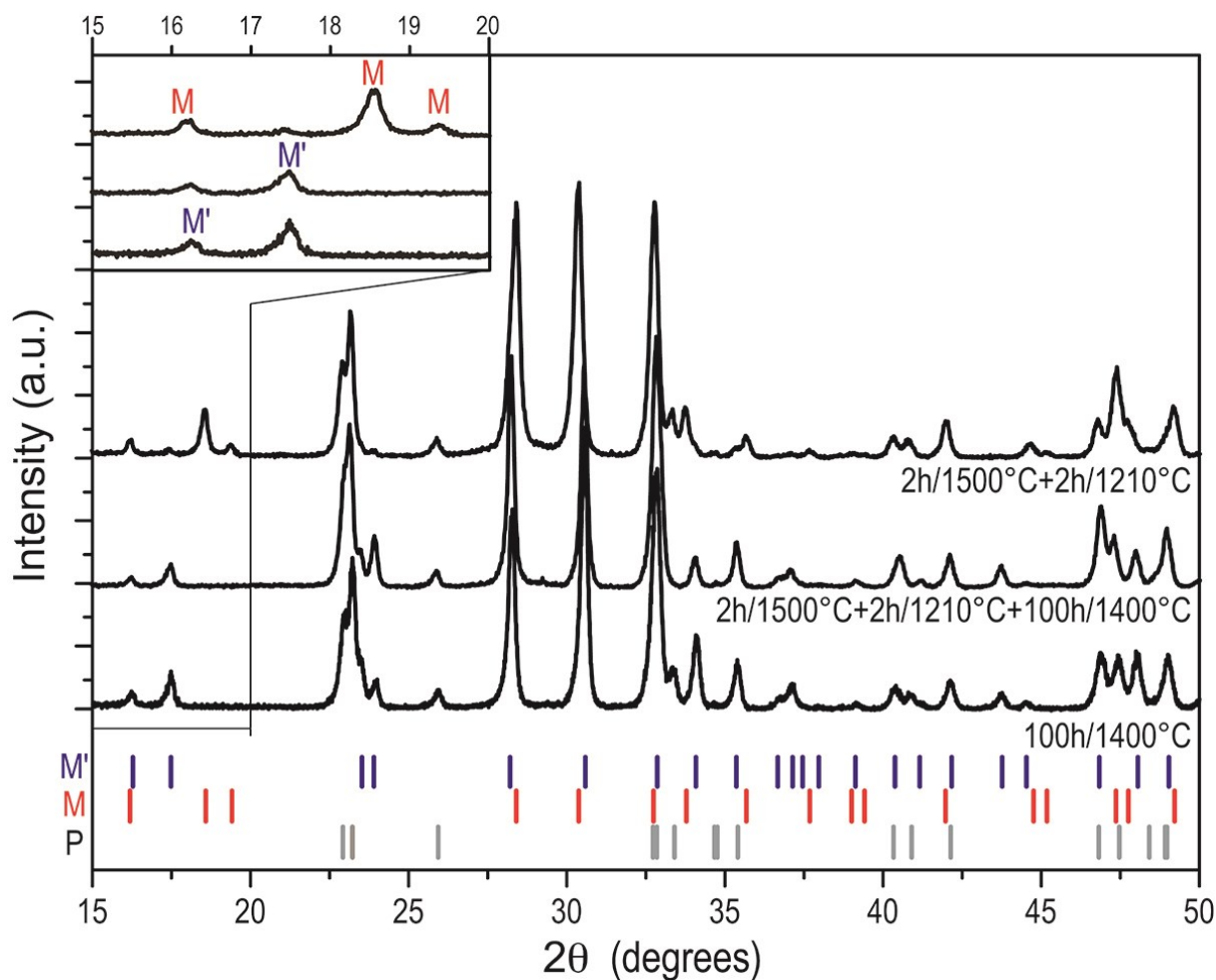
Figure 1. XRD patterns of (i) M' sample heat treated for 2 h at 1500 °C, transforming to T, cooled to 1210 °C and held for 2 h to transform essentially to M , (ii) the sample from (i) then heat treated for 100 h at 1400 °C showing transformation to M', and (iii) a separate sample from the same batch heat treated for 100 h at 1400 °C which remains as M' with no transformation to M. A minor fraction of YTa$_3$O$_9$ was present in all samples but should not affect significantly the nature of the equilibrium phase for YTaO$_4$.

The YTaO$_4$ sample quenched from melt (laser-melted bead) is M phase; however, its diffraction pattern shows very minor additional peaks. In the SEM-BSE image given in Figure 2 a brighter thin layer can be observed at the grain boundaries of the M phase grains. Due to the low fraction of the impurity phase, neither the composition nor the structure could be determined conclusively. However, the contrast in the BSE image indicates that it has a higher Ta content than YTaO$_4$. The twinned grains visible in Figure 2 are characteristic of the M phase resulting from the displacive transformation of T YTaO$_4$ upon cooling [9,17,41].
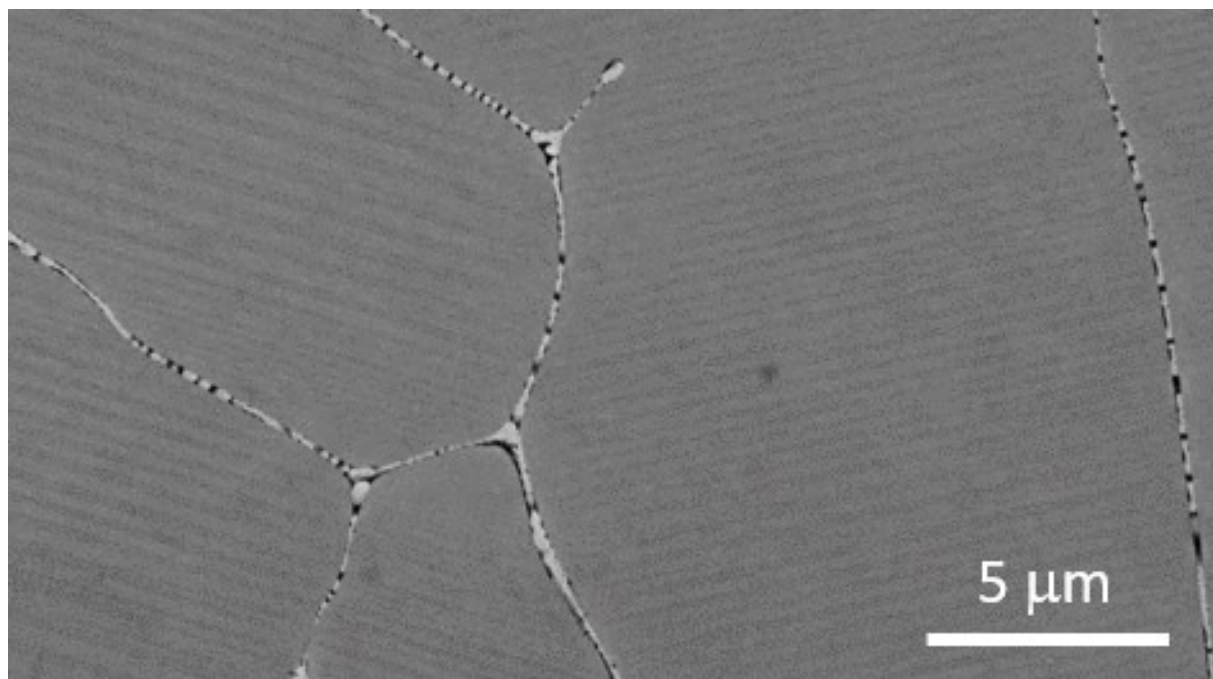

Figure 2: SEM-BSE image of the polished YTaO$_4$ laser melted bead showing the twinned grains characteristic for M YTaO$_4$ and a thin segregated phase along the grain boundaries.

3.2.   Enthalpies of formation and heat capacities of the monoclinic YTaO$_4$ phases

The drop solution enthalpies ΔH_{ds} in sodium molybdate melt at 701 °C of M' and M YTaO$_4$ as well as the drop solution enthalpies of the constituent oxides are given in Table 2. The drop solution enthalpies of M' und M YTaO$_4$ are indistinguishable within experimental error. The enthalpies of formation from the constituent oxides of the two different polymorphs were calculated using the following thermodynamic cycle, where 'sln' indicates the material was dissolved in the sodium molybdate solvent.

$$½\ Y_2O_3\ (25\ ^oC) + ½\ Ta_2O_5\ (25\ ^oC) \rightarrow YTaO_4\ (25\ ^oC) \qquad \Delta H_{f,ox} \qquad (3)$$

$$Y_2O_3\ (25\ ^oC) \rightarrow Y_2O_3\ (sln,\ 701\ ^oC) \qquad \Delta H_{ds}(Y_2O_3) \qquad (4)$$

$$Ta_2O_5\ (25\ ^oC) \rightarrow Ta_2O_5\ (sln,\ 701\ ^oC) \qquad \Delta H_{ds}(Ta_2O_5) \qquad (5)$$

$$\text{YTaO}_4 \, (25 \, ^\circ\text{C}) \rightarrow \text{YTaO}_4 \, (\text{sln, } 701 \, ^\circ\text{C}) \qquad\qquad \Delta H_{ds}(\text{YTaO}_4) \qquad (6)$$

$$\Delta H_{f,ox} = -\Delta H_{ds}(\text{YTaO}_4) + \tfrac{1}{2}\,\Delta H_{ds}(\text{Y}_2\text{O}_3) + \tfrac{1}{2}\,\Delta H_{ds}(\text{Ta}_2\text{O}_5) \qquad (7)$$
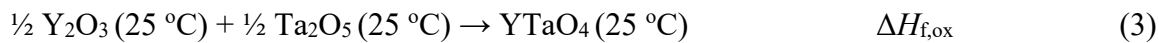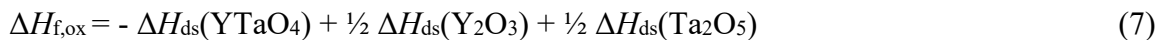
Table 2: Average drop solution enthalpies of M' and M YTaO$_4$ and their constituent binary oxides in sodium molybdate melt at 700 °C and the calculated enthalpies of formation from the oxides at room temperature.

	ΔH_{ds} in kJ/mol	$\Delta H_{f,ox}$ in kJ/mol
Y$_2$O$_3$	-120.74 ± 0.94[a]	
Ta$_2$O$_5$	95.8 ± 3.6[b] (7)	
M' YTaO$_4$	79.1 ± 2.0[b] (13)	-91.6 ± 3.4
M YTaO$_4$	79.3 ± 2.0[b] (10)	-91.8 ± 3.4
T YTaO$_4$	72.4 ± 2.2[c]	-84.9 ± 3.5

[a]   taken from Ushakov *et al.* [51].
[b]   uncertainties are two standard deviations of the mean, values in parentheses give number of calorimetric experiments performed in the present study.
[c]   calculated using the M' to T transformation enthalpy $\Delta H_{tr} = 6.7 \pm 0.4$ kJ/mol measured in this work by DTA.

The measured heat capacities of the two monoclinic polymorphs are plotted in Figure 3(a). A Maier-Kelley function was fitted to the averaged experimental data using the least-squares method resulting in the following functions

$C_p(\text{M'YTaO}_4)$ (J mol^{-1} K^{-1})

$$= (139.7 \pm 0.2) + (0.0211 \pm 0.0002) \cdot T + (-2708250 \pm 22650)\cdot T^{-2} \qquad (8)$$

$C_p(\text{MYTaO}_4)$ (J mol^{-1} K^{-1})

$$= (138.8 \pm 0.2) + (0.0220 \pm 0.0002) \cdot T + (-2891810 \pm 22182)\cdot T^{-2}. \qquad (9)$$

From these data, the enthalpy increment was derived by integrating the C_p polynomials between room temperature and calorimeter temperature of 701 °C which resulted in 97.1 ± 0.3 kJ/mol and 96.4 ± 0.3 kJ/mol for M' phase and M phase, respectively.
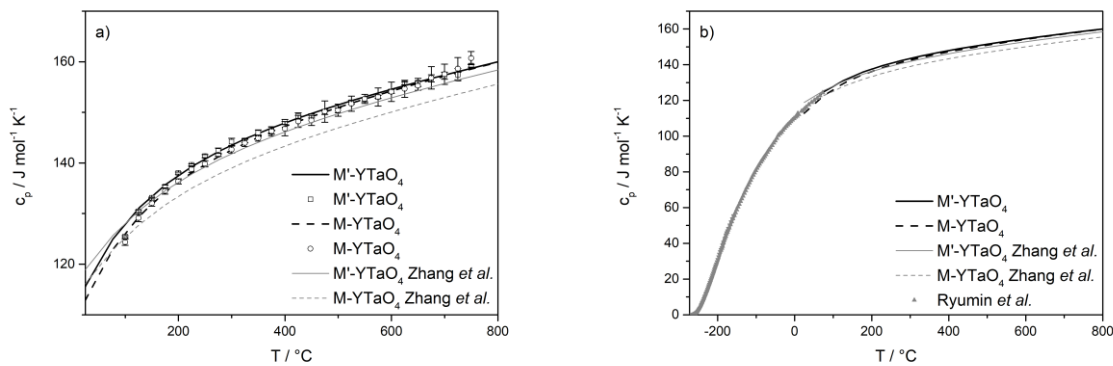
Figure 3: Heat capacity of the two monoclinic polymorphs M' and M of YTaO₄. a) Averaged experimental heat capacities of three measurements with two standard error and Maier-Kelly fit compared to the heat capacities calculated using the CALPHAD assessment [23], b) Maier-Kelly fit of M' and M YTaO₄ of this work compared to experimental low-temperature heat capacity values of M' YTaO₄ measured by Ryumin et al. [28].

In addition, the enthalpy increments (heat contents) from room temperature to the calorimeter temperature (25 to 701 °C) were determined using the same calorimeter setup as for the determination of the drop solution enthalpies without the solvent (transposed temperature experiment). The enthalpy increments of M' YTaO₄ and of M YTaO₄ were 97.8 ± 0.5 kJ/mol and 97.4 ± 1.2 kJ/mol, respectively. Thus, the heat contents determined by the two approaches described are in good agreement with each other and reveal there is no significant difference between the values for the M' and M phase, in agreement with earlier DFT calculations [22,23].

3.3. *Melting and phase transformations of YTaO₄*

To determine the transition temperature and enthalpy of M' YTaO₄ to T YTaO₄, the co-precipitated sample heat treated at 1250 °C was then heated in the DTA to 1700 °C. A small endothermic peak with onset at 1519 ± 5 °C was observed on first heating, as shown in Figure 4. However, heat treatments at 1500 °C show complete transformation of M' to T in two hours. This would imply that the actual equilibrium M'→T transformation temperature is between 1500 °C and 1426 °C (temperature of T→M transformation). The enthalpy change at this temperature was assigned to the M'→T transition and was 6.7 ± 0.4 kJ/mol. No corresponding heat effect could be distinguished on cooling or on second heating.
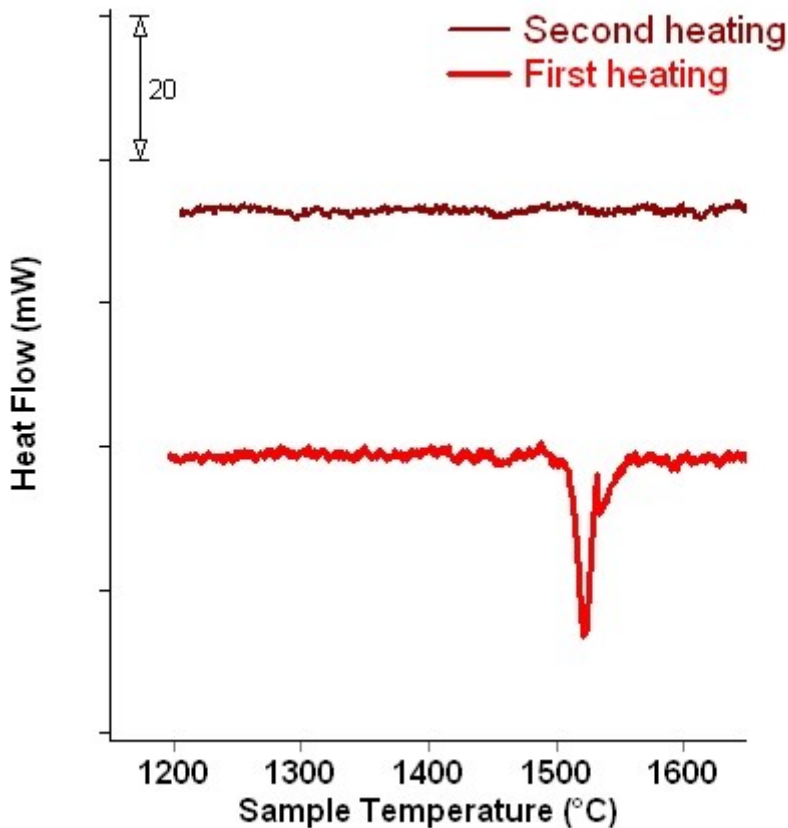
Figure 4: Heat flow on first and second heating of M' YTaO$_4$ sample (baseline subtracted). An endothermic heat effect (6.7 ±0.4 kJ/mol) observed on first heating cycle corresponds to M'-T phase transformation. No peaks in heat flow were distinguished on T-M and M-T transitions on cooling and the second heating cycle, indicating its second order nature.

The melting temperature of YTaO$_4$ was determined as 2090 ± 9 °C by melting two samples, two to three times each. The heat flow curves of the first heating and cooling are given in Figure 5. The onset of solidification on cooling was at 1969 ± 9 °C, indicating a typical undercooling of 120 °C to initiate crystallization. In both studied samples, the changes in heat effect on melting was observed on melting-crystallization cycling in DTA Figure 6(a). The first melting produced largest values of fusion enthalpy with an average of the two samples of 165 ± 24 kJ/mol. The heat effects from integration of the peaks from second and third melting and all crystallization peaks were lower with an average of 110 ± 7 kJ/mol. Characterization of the samples after thermal analysis using SEM showed that the sample segregated into several phases during the experiment, as shown in Figure 6(b). The matrix phase remained YTaO$_4$, however, Ta-rich phases (brighter segregates) as well as a Ta-lean phase (darker segregates) were clearly evident. EDX measurements suggested that the bright Ta-rich regions are YTa$_3$O$_9$ (a perovskite) with precipitates of minor phase somewhat richer in Ta, most likely YTa$_7$O$_{19}$ (hexagonal), whereas the Ta-lean phase is approximately Y$_3$TaO$_7$ (orthorhombic). No reaction product of the sample with the W crucible could be detected.
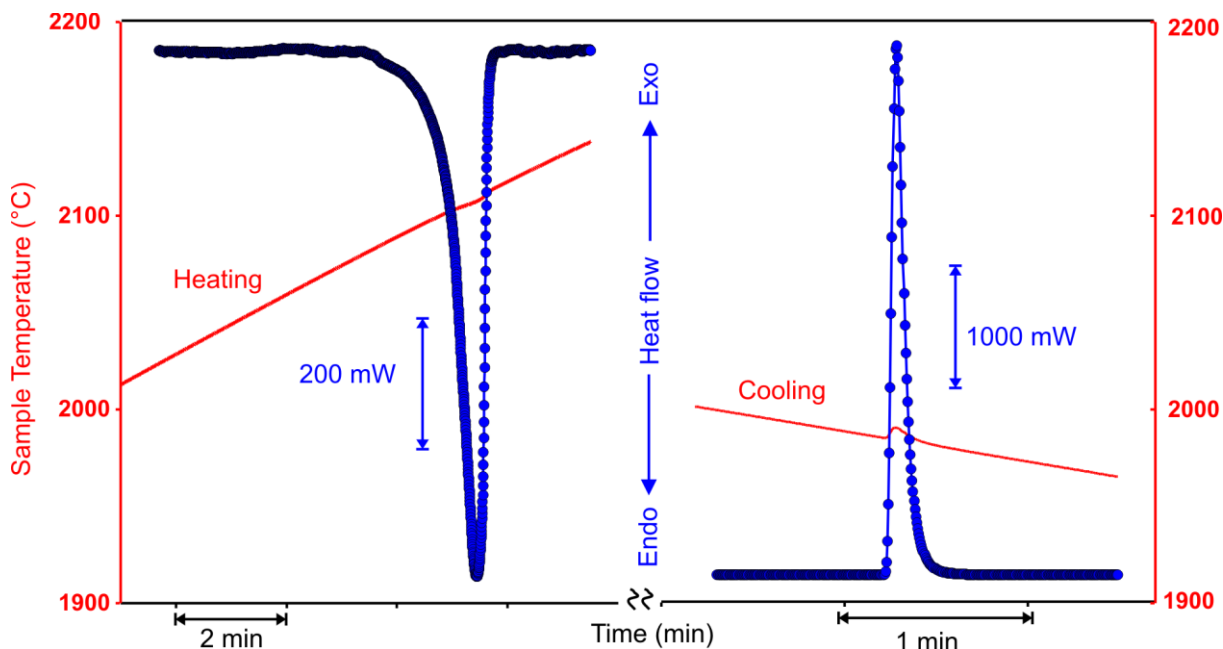
Figure 5: Heat flow traces for the first melting and solidification event of YTaO$_4$ in the DTA (baseline subtracted).

To complement the DTA measurements, cooling traces were recorded to estimate melting temperatures and the enthalpy of fusion was determined using drop-and-catch (DnC) calorimetry on YTaO$_4$ laser-melted beads. The starting samples were confirmed by XRD to be in M phase at room temperature. On cooling from melt, YTaO$_4$ sample showed recalescence peak as shown in Figure 7. No additional thermal arrests were observed in cooling traces. Due to undercooling, the solidification temperature determined from cooling traces on levitated samples is expected to be lower than the melting temperature measured on heating. In our experiments, YTaO$_4$ solidification in oxygen produced the maximum observed recalesecence temperature 2075 $\pm$ 8 °C, which is within uncertainty of melting temperature determined in DTA on heating in Ar in tungsten crucibles (2090 $\pm$ 9 °C). This result render confidence in melting temperature determination by DTA and negates possibility of strong dependence of melting temperature on atmosphere.

The results of DnC calorimetry in oxygen are shown in Figure 8. From the enthalpy difference of the drops of solid samples and liquid samples, the fusion enthalpy was evaluated to be 164 $\pm$ 15 kJ/mol. The uncertainty of $\pm$ 10 % is ascribed to temperature differences within the sample [36]. The fusion enthalpies from DnC and from the first melting in DTA (165 $\pm$ 24 kJ/mol) are in good agreement. The unusually large uncertainty from DTA measurements is related to phase separation observed after melting in tungsten crucibles.
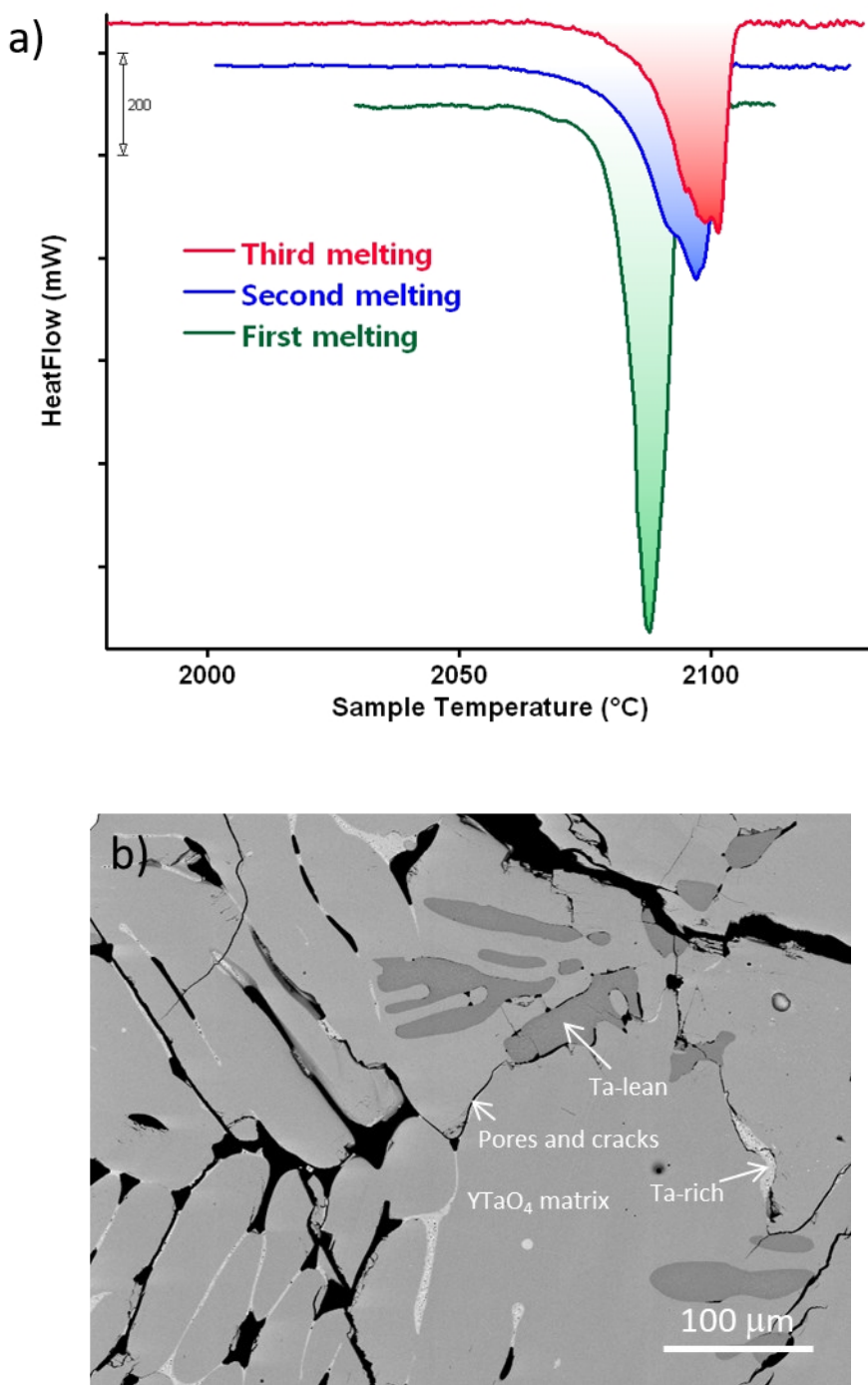
Figure 6: a) Heat flow traces of first, second and third melting of YTaO$_4$ in the DTA (baseline subtracted). Repeated melting of the sample led to substantial variation in the fusion enthalpy; b) SEM-BSE image of a polished DTA sample after the experiment. The sample segregated into several Ta-rich (bright) and –lean (dark) phases, the matrix phase remained YTaO$_4$. No reaction of the sample with the W crucible could be detected.
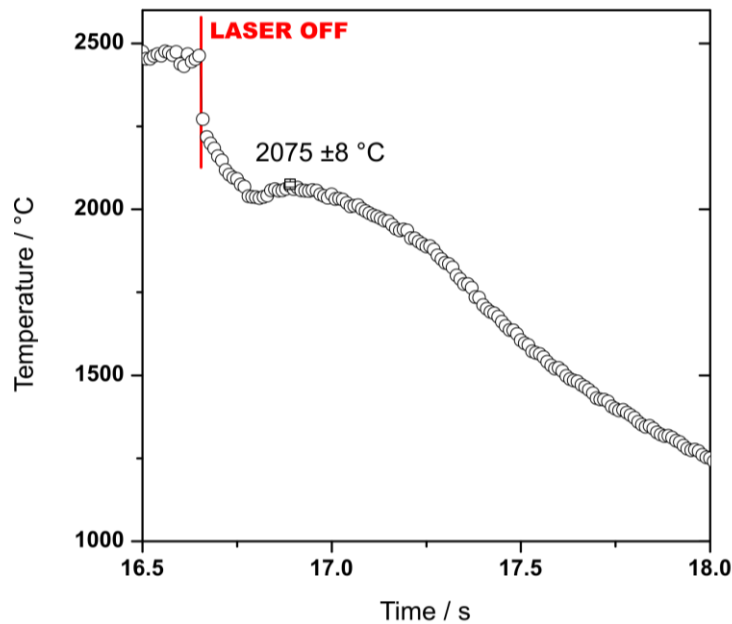
Figure 7: Representative spectropyrometer cooling trace of a YTaO₄ bead levitated in O₂ gas. The solidification temperature was determined from a thermal arrest or from the maximum temperature of a recalescence peak and the average of five measurements was calculated.
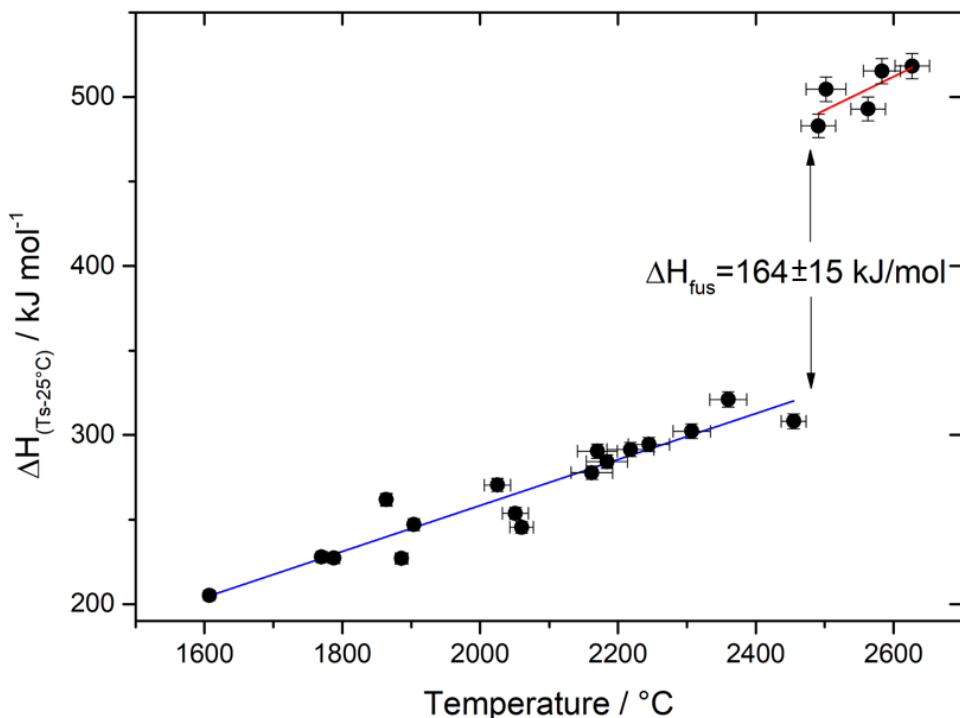

Figure 8: Enthalpy-temperature data from DnC experiments of YTaO₄ laser-melted beads. The uncertainties in temperature come from the spectropyrometer measuring the surface temperature of the YTaO₄ bead, the uncertainties in enthalpy were calculated from the uncertainty in calibration factor reported in [22].

3.4. *Thermal expansion of the tetragonal YTaO$_4$ phase in oxygen to the melting point*

To gain insight into the high temperature phase stabilities and thermal expansion coefficient of the high temperature phase of YTaO$_4$, *in situ* diffraction experiments were performed on laser-melted YTaO$_4$ beads levitated in oxygen flow. Since laser melted YTaO$_4$ crystallizes in T phase and transforms to M phase upon cooling, the thermal expansion of M' could not be investigated using the same approach. The surface temperature measured with a pyrometer (T$_P$) while the laser is on deviates from the average temperature of the diffracting volume and was therefore corrected as described in section 2.3. The background at 2200 and 2300 °C indicates that the sample is partially melted. The melting temperature of YTaO$_4$ was determined to be 2090 ± 9 °C, which means that the temperature of the diffracted volume is about 110 °C lower than the pyrometer temperature, T$_P$, close to melting. This difference is in agreement with previous observations by Pavlik *et al.* [31]. The measured temperatures T$_P$ obtained around the M→T transformation were corrected to fit the respective transition temperature given in the literature [17]. Figure 9 shows the synchrotron X-ray diffraction patterns as a function of the corrected temperature, T$_{corr}$.
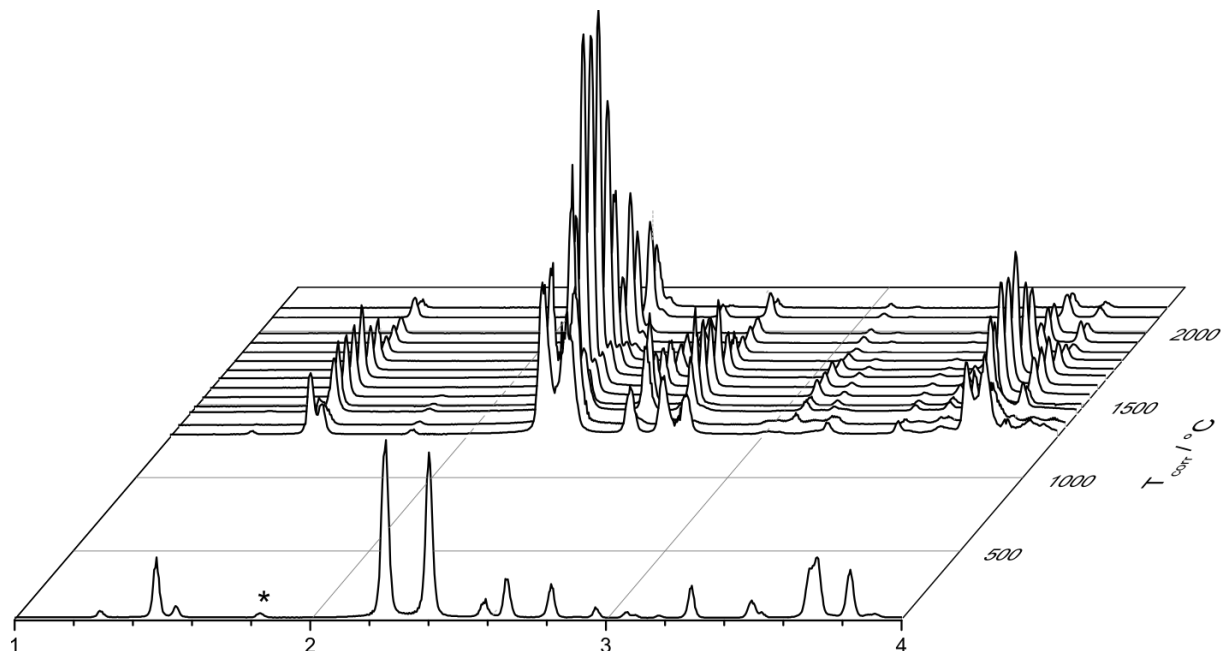

Figure 9: Synchrotron X-ray diffraction patterns of a laser heated YTaO$_4$ bead levitated in O$_2$ gas flow as a function of the corrected temperature T$_{corr}$. The minor additional peak which does not belong to one of the polymorphs of YTaO$_4$ is marked with *.

The evaluated lattice parameters, with a conservative uncertainty of ± 0.01 Å, are plotted against the corrected temperature T$_{corr}$ in Figure 10. The temperature difference of the measured temperature from the temperature of the diffracted volume for Y$_2$O$_3$ was evaluated to be within

100 °C in a previous study [42]. Therefore, an uncertainty of ± 50 °C was included to the corrected temperature in Figure 10. It is evident from the diffraction patterns that the tetragonal high temperature phase, T, persists until melting.

From these measurements, the anisotropic coefficients of thermal expansion of the tetragonal phase can be derived from the lattice parameters obtained by Rietveld refinement. According to equation 1, the linear thermal expansion coefficients for *a* and *c* direction as (8.5 ± 0.6)·10^{-6} K^{-1} and (13.7 ± 0.3)·10^{-6} K^{-1}, respectively. The average coefficient of thermal expansion was derived using equation 2 and was determined to be $\langle \alpha \rangle = 10.4 \cdot 10^{-6}$ K^{-1}. These thermal expansion coefficients are of the same range as reported values of tetragonal t and yttria stabilized t'-ZrO$_2$, but are slightly lower and show thermal expansion anisotropy as well [43,44].
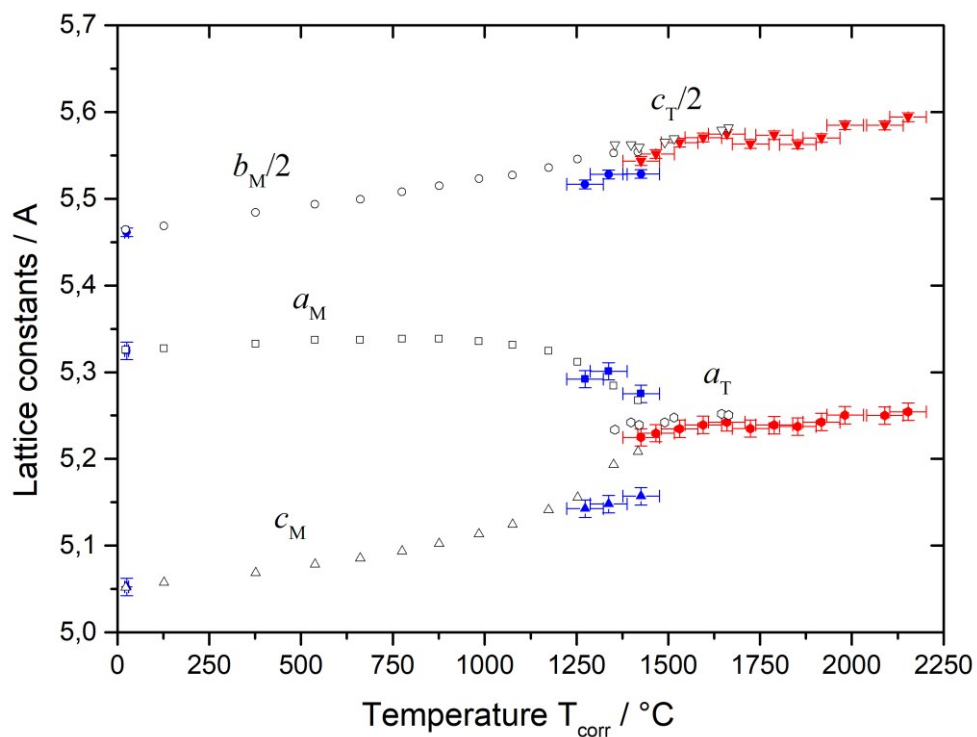

Figure 10: Lattice parameter as a function of the temperature (solid symbols) compared to the previously reported *in situ* high temperature XRD by Shian et al. [17] (open symbols). Lattice parameter of M phase are described with squares for a$_M$, circles for b$_M$/2, and triangles for c$_M$ and of T phase with hexagons for a$_T$ and reverse triangles for c$_T$/2.

4. Discussion.

This work elucidated the phase stability of the different YTaO$_4$ polymorphs and determined their transition temperatures, standard enthalpies of formation, enthalpies and heat capacities

that are essential data for developing an accurate thermodynamic description of systems involving these phases. The binary YO$_{1.5}$-TaO$_{2.5}$ phase diagram incorporating the relevant results from this study is provided in Figure 11 to provide context for some of the topics in the discussion.
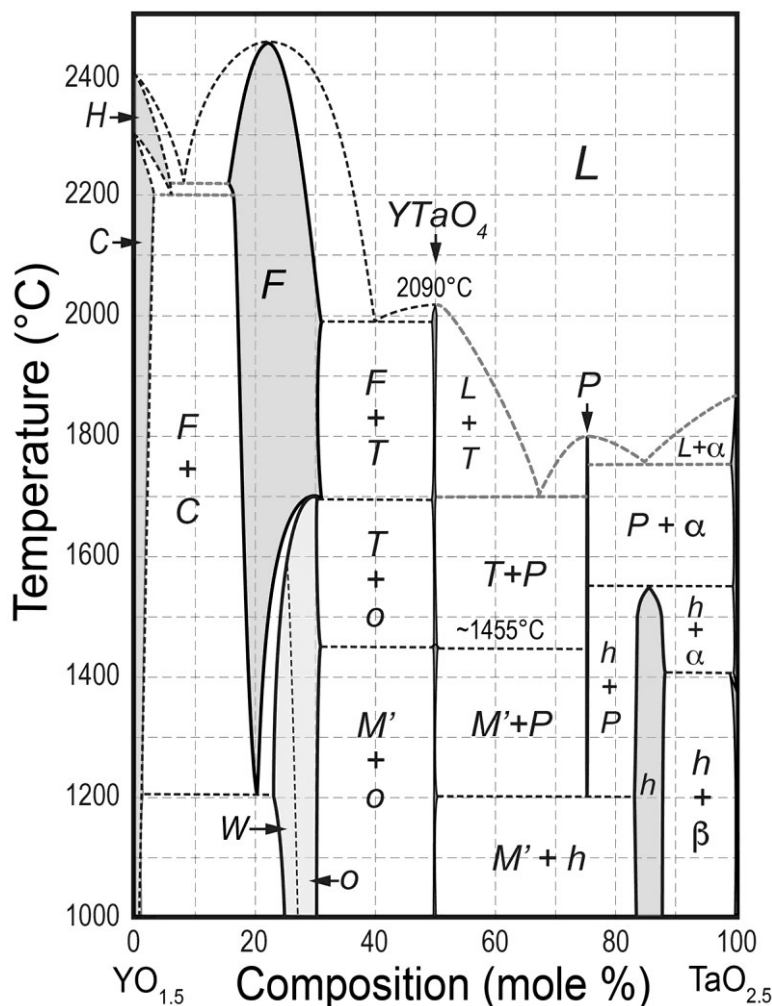

Figure 11. Phase diagram for the YO$_{1.5}$-TaO$_{2.5}$ incorporating critical temperatures for the melting point of T YTaO4 and the transformation from M' to T. Adapted from [25].

4.1. Stability of the YTaO$_4$ polymorphs.

A key outstanding question regarding YTaO$_4$ is the relative stability of the two known monoclinic polymorphs as a function of temperature. This is demonstrably resolved in this work, where M' remains stable after 100 h at 1400 °C, just below the M→T transformation temperature (1426 °C [17]), but M transforms to M' after the same treatment. Coupled with earlier work [1,21,41], it is then concluded that M' is the stable phase at low temperatures. Because the M phase is metastable, the M→T transformation temperature must be lower than the M'→T and since it has been shown that the latter is viable kinetically at 1500 °C its

equilibrium value should be between 1426 and 1500 °C. This is consistent with the report from Brixner et al. [1] that the transformation is in the range 1450 - 1460 °C, which is reflected in the phase diagram in Figure 11. The experimental evidence that M' is the stable phase is in line with results from first principles calculations, wherein M' was found to be slightly more stable than M at 0 K [22,23]. It is instructive, however, to examine the possible sources for the confusion in the literature.

The enthalpies of drop solution and therefore the enthalpies of formation of M' and M YTaO$_4$ were measured for the first time and found to be indistinguishable within experimental error (see Tables 2 and 3). Hence no conclusion on thermodynamic stability can be drawn from this data to further support the statement made above, however, the similarity of the enthalpies is in line with ab initio calculations [22,23]. One may then consider the entropy of both phases to derive the Gibbs energy of the monoclinic polymorphs. A standard molar entropy for M' $S°(M') = 115.6 \pm 0.4$ J/(mol K) has been derived based on cryogenic heat capacity measurements [28], but values for the other phases are not known. Results from this study reveal that the C_p difference between M and M' is small. From the enthalpy and heat capacity data in this work and additional data from the literature [22,23,28,45] it can be concluded that the energy difference M' and M YTaO$_4$, and thus the driving force from a possible M$\leftrightarrow$M' transformation, is small. Nevertheless, the M$\to$ M' transformation does occur at ~1400°C, as shown in this work.

Table 3: Thermochemical data for the different polymorphs of YTaO$_4$ at 25 °C.

	$\Delta H_{f,ox}$ in kJ/mol	$\Delta H_{f,el}$ in kJ/mol[a]	S° in J/(mol K)
M' YTaO$_4$	-91.6 ± 3.4 (this work)	-2067.2 ± 5.5	143.2 [23]
	-67.83 [23]		115.6 ± 0.4 [28]
M YTaO$_4$	-91.8 ± 3.4 (this work)	-2067.4 ± 5.5	
T YTaO$_4$	-84.9 ± 3.5 (this work)	-2060.5 ± 5.5	

[a] calculated from the enthalpies of formation from the constituent oxides of this work and $\Delta_f H$ of the binary oxides Y$_2$O$_3$ and Ta$_2$O$_5$, taken from [52] and [53], respectively.

The kinetic preference for the formation of M upon cooling from the T field is ascribed to the close similarity of their structures [22], which allows for preserving the nearest neighbor arrangement during the displacive transformation [18,22]. In contrast, the T$\to$M' transformation is reconstructive and thus less favorable kinetically, leading to the selection of M [22]. Conversely, the transformation of M' to T or M is reconstructive, but arguably feasible mechanistically since M'$\to$T does occur within reasonable times at temperatures even below

1500 °C (Figure 1). Similarly, the M→M' transformation should be mechanistically feasible if there is a favorable driving force, albeit small.

It has also been suggested elsewhere that T may transform to a fluorite phase prior to melting based on the similarities with the ZrO$_2$ rich end of the ZrO$_2$-YTaO$_4$ quasibinary [12]. This is at variance with the high temperature *in situ* XRD results here, showing that T YTaO$_4$ does not transform to another phase before melting. The absence of a fluorite field in YTaO$_4$ is further supported by the fact that additions of YTaO$_4$ to ZrO$_2$ stabilize the tetragonal field at the expense of the cubic phase [9,27,46]. The addition of YTaO$_4$ to ZrO$_2$ does not add anion vacancies, which would tend to stabilize the fluorite phase. Moreover, the average cation size of Y^{3+} (101.9 pm) and Ta^{5+} (74 pm) in 8-fold coordination is 87.95 pm, not significantly larger than Zr^{4+} (84 pm) and still undersized relative to the oxygen cubic cage in fluorite. Therefore, it is expected that the tetragonal distortion would not be significantly alleviated by the addition of YTaO$_4$. It is also known from studies in the ZrO$_2$-YO$_{1.5}$-TaO$_{2.5}$ system [9] that the fluorite field emerging from the ZrO$_2$ -YO$_{1.5}$ binary is gradually destabilized by the addition of Ta^{5+}. In both cases the limit of stability at 1500 °C is dictated by the appearance of equilibria with the T YTaO$_4$ phase.

4.2.   *Phase transformations*

The transformation temperatures of the YTaO$_4$ polymorphs have been studied in literature but the transition enthalpies are not known and were determined in this paper for the first time. The discrepancy between the M'→T transformation temperature measured by DTA (1519 ± 5 °C) and those reported in the literature [1,11,21] is likely due to the sluggish nature of this transition and the difference in heating rates used (20 °C/min in this work v. 10 °C/min in [11,21]). It is also possible that differences in microstructure, e.g. crystallite size, could have an influence on the transformation kinetics and therefore on the temperatures determined by dynamic measurements.

Based on the similarity of the structures of the YTaO$_4$ polymorphs [1,22], the heat capacity and the heat content of M' and T are expected to be close. Therefore, it is anticipated that the phase transition enthalpy will not have a strong temperature dependence and the measured latent heat of the M'→T transformation (6.7 ± 0.4 kJ/mol) is reliable despite the moderate uncertainty in the transition temperature. The M' to T transformation could only be detected on the first heating cycle, consistent with the alternate transformation to M during cooling [1,18]. The T→M transition is not detected in DTA, and neither is the reverse M→T transformation on heating, in agreement with the proposed second-order nature of that transition

[1,18]. It should be pointed out, that the enthalpies of formation of the different polymorphs are given in Tables 2 and 3 are enthalpies of formation at room temperature. Therefore, there is no contradiction that the formation enthalpies at room temperature of M and T YTaO4 differ.

The agreement between the melting temperature of T YTaO4 measured by DTA (2090 ± 9 °C) and from cooling traces after laser melting (2075 ± 8 °C) is reasonable. These values are in line with the report of Yokogawa and Yoshimura [24], where a value of 2044 ± 50 °C was found also using cooling traces. Both studies showed recalescence and an associated maximum temperature lower than the equilibrium melting temperature due to undercooling associated with growth and effects of heat dissipation to the experimental setup.

To the best of the authors' knowledge, the fusion enthalpy of YTaO4 has not been reported before. Two complementary methods were used in this study to ensure reliability of the data. DTA measurements revealed inconsistencies in the measured fusion enthalpies on repeated melting-crystallization cycles (Figure 6(a)). Post measurement characterization of the samples using SEM showed that the nominally single-phase sample contained several minor segregated phases (Figure 6(b)) within the YTaO4 matrix. One of the segregated phases is Ta-rich (P) whereas the other is Ta-lean (o), while the second (and least abundant) Ta-rich phase (h) results from solid state precipitation from P, as inferred from the phase diagram (Figure 11). Formation of a Ta-rich or a Ta-lean segregate would be generally consistent with the melt being slightly off-stoichiometry, whereupon solidification would occur with Ta enrichment or depletion in the liquid, terminating at the eutectics with the perovskite (P) or fluorite (F) phases, respectively. However, the presence of segregates on both sides of the congruent-melting YTaO4 cannot be readily explained unless the melt were inhomogeneous. One might expect that if there were some volatilization of $TaO_{2.5}$ from the surface there might be different melt compositions on the surface and bulk of the DTA sample, which would result in different solidification paths. In that case, however, the segregates would be in different regions of the sample, but Figure 6(b) clearly shows they are coexisting in the same region and across the entire sample. It is feasible that one of the segregate phases, most likely F/o-Y_3TaO_7, be retained upon remelting leading to a Ta-enriched melt that would then solidify following the path that terminates in the T+P eutectic, but one would expect the morphology of the F/o phase to be different from that of an interdendritic segregate. The shape of the heating curves in Figure 6(a) suggest some of the F phase might be retained if the heating is sufficiently rapid, but since the microstructure in Figure 6(b) went through three consecutive cycles of melting it is not possible to corroborate this hypothesis. One may also consider that Ta^{5+} may be partially reduced to Ta^{4+}, whereupon the solidification path would be in the ternary TaO_2-$TaO_{2.5}$-$YO_{1.5}$ but there is no available

information to assess this scenario. Indeed, whereas the Nb-O system includes stable oxides with lower oxygen content than $NbO_{2.5}$ [47], the Ta-O system shows only a two-phase field between Ta and $TaO_{2.5}$ below the solidus, although it does show a miscibility gap in the liquid phase at low pO_2, with each liquid following a different solidification path [48,49]. There is no evidence, however, that such miscibility gap exists in the liquid upon melting of $YTaO_4$. This issue remains to be resolved by future research, but *it does highlight the importance of understanding the microstructure evolution during thermodynamic measurements in systems where segregate phases evolve during solidification*. The broader implication is that multiple melting cycles of a slightly off-stoichiometric oxide could lead to differences in the temperature and the enthalpy content of the transformation. Therefore, only the value measured during the first melting process is considered reliable as it is consistent with the value determined by DnC calorimetry.

The samples from DnC experiments showed less segregation (Figure 2) and only the P phase, with no evidence of a Ta lean phase, presumably because they were performed under oxygen flow. In addition, the DnC fusion enthalpy of 164 ± 15 kJ/mol has a lower uncertainty than the average from the first DTA cycle on several samples.

4.3. *Experimental thermochemical data for CALPHAD modeling*

The relevance of experimental thermodynamic data for thermodynamic modelling is self-evident and manifested in the difficulties that previous assessments of the quasi-binary $YO_{1.5}$-$TaO_{2.5}$ [23] and quasi-ternary ZrO_2-$YO_{1.5}$-$TaO_{2.5}$ [26] systems. In addition to phase equilibria, thermochemical data are of great importance to correctly model the Gibbs energy of each phase and to set up a self-consistent database.

Comparing the experimental data determined in this work with calculated data from thermodynamic modeling [23], reveals differences in the enthalpies of formation from the constituent oxides of the $YTaO_4$ polymorphs as well as in the heat capacities and transformation enthalpies as depicted in Tables 3 and 4. Experimentally, it was found that the heat capacities of the two monoclinic phases do not differ much in the temperature range investigated and can be described in a first approximation with a Neumann-Kopp approach [50]. Therefore, the heat capacity of the M' phase derived from the thermodynamic description fits well since Zhang et al. [23] used the Neumann-Kopp rule to describe the heat capacities of M' and T, but for the M phase another temperature dependent term has been introduced into the Gibbs energy function of the thermodynamic model [23], resulting in deviations of the calculated heat capacity compared to the measured heat capacity as shown in Figure 3(b). Furthermore, the measured

enthalpies of formation from the constituent oxides are more negative than those calculated from the thermodynamic description [23], as experimental data were not yet available at the time of modelling. Therefore, even if CALPHAD assessment is combined with ab-initio calculations the accuracy of the results is sometimes not sufficient and experimental data is essential to build a trustworthy database. The experimental data presented in this work are essential to re-assess this quasibinary system and all other systems containing the compound YTaO$_4$.

Table 4: Comparison of transition enthalpies of this work with the thermodynamic assessment [23].

	This work	Thermodynamic assessment [23]
$\Delta H_{tr}(M' \rightarrow T)$ in kJ/mol	6.7 ± 0.4	10.6
ΔH_{melt} in kJ/mol	164 ± 15	81.6

5. Conclusions

Complementary high temperature analysis methods provided a deeper understanding of the thermochemistry and phase stabilities of the different polymorphs of YTaO$_4$, and made the reliable determination of their thermodynamic parameters possible. A key question of this work was the determination of the thermodynamic stable low temperature phase. While the standard enthalpies of formation, which generally give a good indication of the stability, of M' and M YTaO$_4$ were indistinguishable within experimental error ($\Delta H_{f,ox}(M') = -91.6 \pm 3.4$ kJ/mol and $\Delta H_{f,ox}(M) = -91.8 \pm 3.4$ kJ/mol), heat treatments just below the M'$\rightarrow$T transformation temperature resolved the question. Due to the well selected heat treatment temperatures, it was found that M' is the thermodynamically stable room temperature phase and M is a metastable phase. Furthermore, the transformation enthalpy of M' to T, measured using DTA, of $\Delta H_{tr}(M' \rightarrow T) = 6.7 \pm 0.4$ kJ/mol was reported for the first time. With further heating, the high temperature T phase does not transform to a fluorite-related phase but melts congruently, with an enthalpy of fusion of 164 ± 15 kJ/mol. The phase transformation temperatures found in this work are generally in agreement with earlier reported values. These findings all contribute to a better understanding of the phase equilibria of YTaO$_4$ and the ZrO$_2$-Y$_2$O$_3$-Ta$_2$O$_5$ system in general. The thermodynamic parameters are valuable input for thermodynamic modeling of the materials systems of interest for next generation TBC applications.

Declaration of interests

The authors declare that they have no known competing financial interests or personal relationships that could have appeared to influence the work reported in this paper.

Author Contributions

M. Lepple: Conceptualization, Investigation, Resources, Data Curation, Writing – Original Draft, Visualization, Project Administration, Funding Acquisition

S.V. Ushakov: Investigation, Data Curation, Writing – Original Draft, Writing – Review & Editing, Visualization

K. Lilova: Investigation, Data Curation, Writing – Review & Editing

C.A. Macauley: Resources, Investigation, Writing – Review & Editing

A.N. Fernandez: Resources

C.G. Levi: Writing – Review & Editing, Supervision, Funding acquisition

A. Navrotsky: Resources, Writing – Review & Editing, Supervision, Funding acquisition

References

[1]   L.H. Brixner, On the Structural and Luminescent Properties of the M′ LnTaO[sub 4] Rare Earth Tantalates, J. Electrochem. Soc. 130 (1983) 2435.

[2]   I. Arellano, M. Nazarov, C.C. Byeon, E.-J. Popovici, H. Kim, H.C. Kang, D.Y. Noh, Luminescence and structural properties of Y(Ta,Nb)O4:Eu3+,Tb3+ phosphors, Materials Chemistry and Physics 119 (2010) 48–51.

[3]   R.A. Russell, P.P. Phulé, Chemical synthesis of tantalum zirconate from alkoxide precursors, Materials Science and Engineering: B 21 (1993) 88–93.

[4]   N. I. Leonyuk, E. Cavalli, G. Calestani, N. V. Kuleshov, J. M. Dawes, V. V. Maltsev, E. V. Koporulina, E. A. Volkova, O. V. Pilipenko, A new generation of nonlinear optical and laser crystals of rare earth borate and tantalate families, Journal of Optoelectronics and Advanced Materials 9 (2007) 1206–1214.

[5]   B.W. King, J. Schultz, E.A. Durbin, W.H. Duckworth, Some Properties of the Tantala System.

[6]   J.T.S. Irvine, D.P. Fagg, J. Labrincha, F.M.B. Marques, Development of novel anodes for solid oxide fuel cells, Catalysis Today 38 (1997) 467–472.

[7]   D.P. Fagg, J.T.S. Irvine, The optimisation of mixed conduction in potential S.O.F.C. anode materials, Ionics 4 (1998) 61–71.

[8]   F.M. Pitek, C.G. Levi, Opportunities for TBCs in the ZrO2–YO1.5–TaO2.5 system, Surface and Coatings Technology 201 (2007) 6044–6050.

[9]   C.A. Macauley, A.N. Fernandez, C.G. Levi, Phase equilibria in the ZrO2-YO1.5-TaO2.5 system at 1500 °C, Journal of the European Ceramic Society 37 (2017) 4888–4901.

[10]   C.A. Macauley, A.N. Fernandez, J.S. van Sluytman, C.G. Levi, Phase equilibria in the ZrO2-YO1.5-TaO2.5 system at 1250 °C, Journal of the European Ceramic Society 38 (2018) 4523–4532.

[11]   Q. Flamant, M. Gurak, D.R. Clarke, The effect of zirconia substitution on the high-temperature transformation of the monoclinic-prime phase in yttrium tantalate, Journal of the European Ceramic Society 38 (2018) 3925–3931.

[12]   M. Gurak, Q. Flamant, L. Laversenne, D.R. Clarke, On the Yttrium Tantalate – Zirconia phase diagram, Journal of the European Ceramic Society 38 (2018) 3317–3324.

[13]   J. Wang, Y. Zhou, X. Chong, R. Zhou, J. Feng, Microstructure and thermal properties of a promising thermal barrier coating: YTaO4, Ceramics International 42 (2016) 13876–13881.

[14] A.M. Limarga, S. Shian, R.M. Leckie, C.G. Levi, D.R. Clarke, Thermal conductivity of single- and multi-phase compositions in the ZrO2–Y2O3–Ta2O5 system, Journal of the European Ceramic Society 34 (2014) 3085–3094.

[15] P. Wu, M. Hu, L. Chen, W. Chen, X. Chong, H. Gu, J. Feng, Investigation on microstructures and thermo-physical properties of ferroelastic (Y1-xDyx)TaO4 ceramics, Materialia 4 (2018) 478–486.

[16] J. Feng, S. Shian, B. Xiao, D.R. Clarke, First-principles calculations of the high-temperature phase transformation in yttrium tantalate, Phys. Rev. B 90 (2014) 94102.

[17] S. Shian, P. Sarin, M. Gurak, M. Baram, W.M. Kriven, D.R. Clarke, The tetragonal–monoclinic, ferroelastic transformation in yttrium tantalate and effect of zirconia alloying, Acta Materialia 69 (2014) 196–202.

[18] G.M. Wolten, The structure of the M'-phase of YTaO4, a third Fergusonite polymorph, Acta Cryst. 23 (1967) 939–944.

[19] V.S. STUBIČAN, High-Temperature Transitions in Rare-Earth Niobates and Tantalates, Journal of the American Ceramic Society 47 (1964) 55–58.

[20] A.I. Komkov, The structure of natural fergusonite, and of a polymorphic modification.

[21] S.A. Mather, P.K. Davies, Nonequilibrium Phase Formation in Oxides Prepared at Low Temperature: Fergusonite-Related Phases, Journal of the American Ceramic Society 78 (1995) 2737–2745.

[22] S.G. Heinze, A.R. Natarajan, C.G. Levi, A. van der Ven, Crystallography and substitution patterns in the ZrO2−YTaO4 system, Phys. Rev. Materials 2 (2018).

[23] F. Zhang, G. Zhang, L. Yang, Y. Zhou, Y. Du, Thermodynamic modeling of YO1.5-TaO2.5 system and the effects of elastic strain energy and diffusion on phase transformation of YTaO4, Journal of the European Ceramic Society 39 (2019) 5036–5047.

[24] Y. Yokogawa, M. Yoshimura, High-Temperature Phase Relations in the System Y2O3-Ta2O5, Journal of the American Ceramic Society 74 (1991) 2077–2081.

[25] A.N. Fernandez, C.A. Macauley, D. Park, C.G. Levi, Sub-solidus phase equilibria in the YO1.5-TaO2.5 system, Journal of the European Ceramic Society 38 (2018) 4786–4798.

[26] A.K. Bhattacharya, V. Shklover, W. Steurer, G. Witz, H.-p. Bossmann, O. Fabrichnaya, Ta2O5–Y2O3–ZrO2 system: Experimental study and preliminary thermodynamic description, Journal of the European Ceramic Society 31 (2011) 249–257.

[27] D.-J. Kim, T.-Y. Tien, Phase Stability and Physical Properties of Cubic and Tetragonal ZrO2 in the System ZrO2–Y2O3–Ta2O5, Journal of the American Ceramic Society 74 (1991) 3061–3065.

[28] M.A. Ryumin, E.G. Sazonov, V.N. Guskov, G.E. Nikiforova, P.G. Gagarin, A.V. Guskov, K.S. Gavrichev, L.K. Baldaev, I.V. Mazilin, L.N. Golushina, Low-temperature heat capacity of yttrium orthotantalate, Inorganic Materials 52 (2016) 1149–1154.

[29] S.V. Ushakov, A. Shvarev, T. Alexeev, D. Kapush, A. Navrotsky, Drop-and-catch (DnC) calorimetry using aerodynamic levitation and laser heating, J Am Ceram Soc. 100 (2017) 754–760.

[30] B.H. Toby, R.B. von Dreele, GSAS-II: the genesis of a modern open-source all purpose crystallography software package, Journal of Applied Crystallography 46 (2013) 544–549.

[31] A. Pavlik, S.V. Ushakov, A. Navrotsky, C.J. Benmore, R.J.K. Weber, Structure and thermal expansion of Lu2O3 and Yb2O3 up to the melting points, Journal of Nuclear Materials 495 (2017) 385–391.

[32] S.J. McCormack, A. Tamalonis, R.J.K. Weber, W.M. Kriven, Temperature gradients for thermophysical and thermochemical property measurements to 3000 °C for an aerodynamically levitated spheroid, The Review of scientific instruments 90 (2019) 15109.

[33] Q.-J. Hong, S.V. Ushakov, D. Kapush, C.J. Benmore, R.J.K. Weber, A. van de Walle, A. Navrotsky, Combined computational and experimental investigation of high temperature thermodynamics and structure of cubic ZrO2 and HfO2, Scientific Reports 8 (2018) 14962.

[34] P.S. Maram, S.V. Ushakov, R.J.K. Weber, C.J. Benmore, A. Navrotsky, Probing disorder in pyrochlore oxides using in situ synchrotron diffraction from levitated solids– A thermodynamic perspective, Scientific Reports 8 (2018) 10658.

[35] S.V. Ushakov, P.S. Maram, D. Kapush, A.J. Pavlik, M. Fyhrie, L.C. Gallington, C.J. Benmore, R. Weber, J.C. Neuefeind, J.W. McMurray, A. Navrotsky, Phase transformations in oxides above 2000°C: experimental technique development, Advances in Applied Ceramics 117 (2018) 82-89.

[36] M. Fyhrie, Q.-J. Hong, D. Kapush, S.V. Ushakov, H. Liu, A. van de Walle, A. Navrotsky, Energetics of melting of Yb2O3 and Lu2O3 from drop and catch calorimetry and first principles computations, The Journal of Chemical Thermodynamics 132 (2019) 405–410.

[37]   W.J. Boettinger, U.R. Kattner, K.-W. Moon, J.H. Perepezko, Chapter Five - DTA and Heat-Flux DSC Measurements of Alloy Melting and Freezing, in: J.-C. Zhao (Ed.), Methods for phase diagram determination, Elsevier, Amsterdam, 2007, pp. 151–221.

[38]   G. Della Gatta, M.J. Richardson, S.M. Sarge, S. Stølen, Standards, calibration, and guidelines in microcalorimetry. Part 2. Calibration standards for differential scanning calorimetry* (IUPAC Technical Report), Pure and Applied Chemistry 78 (2006) 1455–1476.

[39]   A. Navrotsky, Progress and new directions in high temperature calorimetry, Phys Chem Minerals 2 (1977) 89–104.

[40]   A. Navrotsky, Progress and new directions in high temperature calorimetry revisited, Phys Chem Min 24 (1997) 222–241.

[41]   J. Graham, Crystal chemistry of complex niobium and tantalum oxides III. Relationship between M, T, and M' fergusonite structure, American Mineralogist 59 (1974) 1045–1046.

[42]   S.V. Ushakov, A. Navrotsky, D.J. Green, Experimental Approaches to the Thermodynamics of Ceramics Above 1500°C, J. Am. Ceram. Soc. 95 (2012) 1463–1482.

[43]   R.N. Patil, E.C. Subbarao, Axial thermal expansion of ZrO 2 and HfO 2 in the range room temperature to 1400°C, J Appl Crystallogr 2 (1969) 281–288.

[44]   J.A. Krogstad, Y. Gao, J. Bai, J. Wang, D.M. Lipkin, C.G. Levi, In Situ Diffraction Study of the High-Temperature Decomposition of t′ -Zirconia, J. Am. Ceram. Soc. 98 (2015) 247–254.

[45]   A.V. Khoroshilov, A.A. Ashmarin, V.N. Guskov, E.G. Sazonov, K.S. Gavrichev, V.M. Novotortsev, Heat Capacity and Thermal Expansion of Yttrium Tantalate, Dokl Phys Chem 484 (2019) 12–14.

[46]   P. Li, I.-W. Chen, J.E. Penner-Hahn, Effect of Dopants on Zirconia Stabilization-An X-ray Absorption Study: III, Charge-Compensating Dopants, J Am Ceram Soc. 77 (1994) 1289–1295.

[47]   K. NAITO, T. MATSUI, Review on phase equilibria and defect structures in the niobium-oxygen system, Solid State Ionics 12 (1984) 125–134.

[48]   S.P. Garg, N. Krishnamurthy, A. Awasthi, M. Venkatraman, The O-Ta (oxygen-tantalum) system, Journal of phase equilibria 17 (1996) 63–77.

[49]   H.S. Hong, K.S. Lee, Thermodynamic evaluation of the Ta–O system from pure tantalum to tantalum pentoxide, Journal of Alloys and Compounds 360 (2003) 198–204.

[50]   M. Lepple, K. Lilova, C.G. Levi, A. Navrotsky, Enthalpies of formation of the solid solutions of ZrxY0.5−x/2Ta0.5−x/2O2 (0 ≤ x ≤ 0.2 and 0.65 ≤ x ≤ 1), J. Mater. Res. 34 (2019) 3343–3350.

[51]   S.V. Ushakov, K.B. Helean, A. Navrotsky, L.A. Boatner, Thermochemistry of rare-earth orthophosphates, Journal of Materials Research 16 (2001) 2623–2633.

[52]   R.A. Robie, B.S. Hemingway, J.R. Fisher, Thermodynamic Properties of Minerals and Related Substances at 298.15 K and 1 Bar (1^5 Pascals) Pressure and Higher Temperatures, Washington D.C., 1979.

[53]   Chase, M. W. National Institute of Standards, Technology, NIST-JANAF thermochemical tables, American Chemical Society and American Institute of Physics for the National Institute of Standards and Technology, Washington and D.C. and Woodbury and N.Y, 1998.